Density Functional Theory Calculations of Optoelectronic Properties of Individual and Encapsulated Magnesium-Porphyrin in Carbon Nanotubes for Organic Nano-Hybrid Solar Cells

Anass El Fatimy, Oussama Boutahir, Brahim Fakrach, Mourad Boutahir, José Mejía-López, Abdelali Rahmani, Hassane Chadli, Konstantinos Termentzidis, Abdelhai Rahmani

DFT calculations of optoelectronic properties of individual and encapsulated Mg-Porphyrin in carbon nanotubes for organic nano-hybrid solar cells

Anass El fatimy,[†] Oussama Boutahir,[†] Brahim Fakrach,[†] Mourad Boutahir,[*,‡,†,¶] José Mejía-López,[‡] Abdelhai Rahmani,[†] Hassane Chadli,[†] konstantinos Termentzidis,[§] and Abdelali Rahmani[†]

[†]*Laboratoire d'Etude des Matériaux Avancés et Applications, Université Moulay Ismail, Faculté des Sciences Meknes, Morocco*

[‡]*Centro de Investigación en Nanotecnología y Materiales Avanzados CIEN-UC, Facultad de Física, Pontificia Universidad Católica de Chile. Cedenna, Santiago, Chile*

[¶]*Ecole Normale Supérieure, Département des Sciences, Université Moulay Ismail, Meknes, Morocco*

[§]*Laboratoire CETHIL UMR 5008, CNRS, INSA of Lyon, Un. Claude-Bernard Lyon 1, INSA de LYON 9 Rue de la Physique 69100, FRANCE.*

E-mail: mourad.boutahir@umi.ma

Abstract

The performance of organic solar cells has significantly increased in recent years thanks to thin-film processing, fine-tuning of morphology, and optimization of device manufacture. A focus has been placed on designing low-band gap materials. Herein,

porphyrins have shown great features in optical and electronic fields. In this paper, encapsulating one molecule of magnesium porphyrin into a semiconducting single-walled carbon nanotube (17.0) has been reported, considering this nano-hybrid system as the active layer in the solar cell device. Using density functional theory, we have explored the optoelectronic properties of the isolated Mg-Py molecules and two distinct arrangements of the hybrid system that contains a single Mg-Py molecule inserted into nanotubes. The study demonstrates that the structure is stable due to a charge transfer between the Mg-Py molecules and the nanotube. After encapsulation, we notice a change in nanotube's fermi level position, which is compatible with a charge transfer link between Mg-Py and the nanotube. The outcomes illustrate that the encapsulated systems expressing type II heterojunctions are likely to make them a strong candidate for use as charge carriers and light absorbers in the active layer, which can help create highly effective filled SWNT-based OSCs.

INTRODUCTION

Photovoltaic cells (PVCs) or photovoltaic solar cells,[1] has experienced numerous rounds of development, with each new generation bringing about improvements in performance, cost, and efficiency. Crystalline silicon was used to create the first generation of PVCs, which were created in the 1950s and are still the most popular kind of solar cell today. The efficiency of first-generation solar cells ranges from 15% to 22%, with some advanced designs achieving up to 26%.When it comes to the second generation of PVCs, which were created in the 1980s and 1990s, thin-film technologies like cadmium telluride (CdTe) and copper indium gallium selenide are used (CIGS). These thin-film solar cells may be made at lower cost than traditional silicon-based cells, but they typically have lower efficiencies, often between 10% and 20%. In this context, the study field of third-generation PVCs, which comprises a number of cutting-edge technologies including perovskites, organic PVs, and quantum dot PVs, is still relatively new and evolving. These technologies have the potential to be more

efficient and cost-effective than previous generations. Nevertheless, their performance and commercial feasibility are currently constrained by a number of problems. The following are some of the key problems with organic solar cells: Poor efficiency, low stability, and short lifetime, especially when exposed to oxygen, moisture, and light.[2–5]

Herein, the literature has reported on the encapsulation of various guest species, such as organic molecules, inside single-walled carbon nanotubes (SWCNTs). This marks an exciting advancement in the nano-engineering of novel materials and composites. It has been shown that the encapsulated composites maintain their optoelectronic characteristics,[6–8] which prove useful for nanotechnology and next-generation photovoltaic solar cells(PSCs), such as organic solar cells (OSCs). In addition, the encapsulated species may be able to provide high-energy electrostatic environments for intra-tubular conductance and lower band gaps by the electronic interaction energy between the intra-face of the nanotubes and the encapsulated assemblies based on their chemistry and electrostatic interactions.[9,10] Furthermore, alternative materials OSCs based on nano-hybrid systems have generated a lot of interest due to their accessibility, adaptability, light weight, semi transparency, and ease of manufacture.[11–13] With the advancement of materials and interface engineering, this technology is constantly expanding and leading to increased efficiency, with the power conversion efficiency (PCE) for OSCs topping 18%.[14–16] In comparison to other OSC architectures, the majority of research is being done on donor-acceptor bulk heterojunctions (BHJs). In BHJs, the photoactive layer is created by combining two semiconductors: an electron-donating (conjugated polymer) that is strongly light-absorbing and an electron-accepting, typically a fullerene derivative, that is placed as the active layer and sandwiched between two electrodes. Despite the significant advancements made for these typical combinations (conjugated polymer/fullerene), which enabled a PCE of about 11.5%,[17] their performance is ultimately constrained by (i) the intrinsic deficiencies of the fullerene family, including feeble absorption in the solar spectrum region, (ii) optoelectronic tunability, (iii) low charge mobility which is caused by the hopping transport, and (iv) thermal instability.[18–20]

Nowdays, many recent studies includes efforts to replace fullerene with semiconducting SWNTs, which are beneficial in terms of optical absorbance and bandgap tunability, and which could be extremely important for the development of solar technologies due to their high efficiency and long-term stability,[21–25,25] they are anticipated to find a prominent spot to replace fullerenes in the active layer in conjunction with semiconducting polymers. In order to increase the transport in the polymer blend and to increase OSC stability and efficiency,[16,26] aryl functional groups were integrated into MWCNTs to create poly (3-hexyl thiophene, or P3HT): MWCNTs and PCBM were combined to create a photoactive layer,[27] which increased PCE by up to 2.0%. Authors argued that the carrier transportation and exciton dissociation were improved using a percolation network based on MWCNTs. On the other side, PC71BM-made SWCNT cells[28–32] have been proposed to be generally more effective than those from C_{60} because they absorb a large spectra of light frequencies.[33–35] Here, we introduce porphyrin filled by magnesium atom (Mg), to the active components of organic solar cells to enhance their functionality and thermal stability. As it is known that porphyrins are crucial pigments in natural light-harvesting systems because of their strong redox capabilities and effective light absorption qualities. The usage of porphyrins in photovoltaic (PV) devices has received substantial research because biosystems successfully utilize porphyrin and porphyrin derivatives for the utilization of solar energy.[36–39] Furthermore, since porphyrin has a wide conjugated plane and significant absorption in visible light region as well as in ultraviolet range, it has shown great potential in serving as an essential building element for producing donor materials with reduced bandgap. Porphyrin-based donor materials have been shown to assist small molecule, tandem, ternary, flexible, and OSC/perovskite hybrid solar cells in achieving a number of record-high device efficiencies.[40] Other intrinsic benefits of porphyrin and its derivatives make them suitable candidates for OSCs. First, The molecules exhibit a large absorption region and high extinction factors, indicating their high efficiency in absorbing light at specific wavelengths. This property enhances the fill factor, which defines the efficiency of a photovoltaic device in converting

available light into electrical power. As a result, the device can convert a significant portion of the absorbed light into usable energy. Second, their characteristics are easily tuneable by adding various functional groups to the meso or β locations of the porphyrin, or modification to the main metal ion. Third, the huge conjugated plane makes $\pi - \pi$ stacking and Charge transport to benefit by intermolecular charge transfer. Last but not least, prolonged sun exposure benefits from porphyrin's high degree of stability.

The porphyrins have the ability to effectively absorb light in the near-infrared (NIR) area; therefore, could be useful in organic solar cells (OSCs) that operate in this wavelength range. The porphyrin with empty core encased into semiconducting single-walled carbon nanotube (17.0) (SWNT17) have shown an outstanding photoabsorption uv-visible spectrum and an interesting short bandgap of around 0.5eV, owing this nano-hybrid to be the key material for PVC. Subsequently, we concentrated on a single chain of magnesium porphyrin (Mg-Py) molecules encapsulated in SWNT17 to take use of these filled nanohybrid systems' advantageous properties as active layer materials for OSCs. First, in Section 2 the computational method is given. Section 3 is divided in two parts: first, the optoelectronic features of the isolated Mg-Py molecules are computed, following the optical and electrical characteristics ofthe prestine SWNT17, Mg-Py@SWNT17 and Mg-Py2@SWNT17 nano-hybrid systems. Finally, the article finishes with the main conclusion of the current study.

COMPUTATIONAL METHOD

On the basis of the density functional theory (DFT),[41,42] first-principles calculations were used to determine the physical properties of the Mg-Py molecule enclosed within SWNT17s. We used a plane-wave basis set and projector-augmented waves with the Vienna ab initio Simulation Package (VASP).[43] We conducted DFT calculations, utilizing the generalized gradient approximation (GGA)[44] level of theory, to analyze the geometries and optoelectronic properties of both pristine SWNT17s and the hybrids. The kinetic energy cutoff for the wave

function expansion was chosen to be 520 eV. Nevertheless, the GGA functional does not accurately reflect quantum electronic interactions in regions with low electron concentrations, which results a poor representation of the dispersion or vdW forces. Herein, using Grimme's method,[45] the vdW interaction between the Mg-Py and SWNT17 tube (ie, the GGA plus vdW) has been corrected. We selected two distinct configurations for the Mg-Py molecule, namely the horizontal and vertical orientation, as shown in Figure 1. Next, we employed noncovalent functionalization and utilized a model system in which the Mg-Py molecule is enclosed within a SWNT17 in two characteristic configurations, as illustrated in Figure 2 : (i) Mg-Py@SWNT17, in which the frontal plan of the molecule is positioned vertically to the axis of the nanotube (figure2-(A)); (ii) Mg-Py2@SWNT17, in which the horizontal plane of the molecule is positioned parallel to the axis of the nanotube (figure2-(B)). We have developed a hybrid technique that merges the density functional theory and molecular mechanics. This approach allowed us to construct a dynamic model of Mg-Py@SWNT17. We conducted total energy minimization on this hybrid system to obtain a stable structure with an optimal tube diameter. In Figure 3, we have plotted the Lennard-Jones potential of Mg-Py@SWNT17 against varying tube diameters, ranging from 14 to 25 $\AA$. Our observations reveal that the potential has a minimum value at 15 $\AA$, which corresponds to the equilibrium distance between the SWNT and Mg-Py molecule.

RESULTS

Electronic and optical computations of isolated Mg-Py molecule

Numerous experimental and theoretical research[46,47] have focused on the electronic characteristics of porphyrins and metallo-porphyrins because they are crucial to many energetic processes. Magnesium porphyrin molecule, which has an atom of magnesium at its center, is the most basic metallo-porphyrin.

As a starting point, we need to have a clear understanding of the normal behavior of Mg-

Py molecules in order to appropriately interpret our computed physical characteristics in hybrid nano-systems. In this context the optoelectronic distributions, including total density of states (TDOS), absorption spectra, dielectric functions, and reflectivity of isolateds Mg-Py molecule have been estimated using two different states of xc functional(GGA and HSE06), under DFT using VASP software as mentioned in the previous section, to be able to manipulate this molecule in OSCs and enhance their functionality and lifetime stability. The electronic propertiess such as Fermi energy (FE), bandgap energy (E_G), highest occupied (HO) and lowest unoccupied (LU) molecular orbitals with two xc functionals (GGA and HSE06) are given in table1. The Mg-Py molecule's Fermi level position downshifts after transiting from the GGA to HSE06 functional, and this downshift corresponds to the energies -4.73 and -5.11 eV for GGA and HSE06, respectively.

The difference between HO and LU for the pure Mg-Py molecule using the GGA functional may be clearly demonstrated to be smaller than that at HSE06 xc functional with regard to the HO-LU gap. At the gradient generalized approximation (GGA), the Mg-Py molecule exhibits E_G of around 1.99 eV, and 2.54 eV using HSE06 functional. Compared to these, there is a rough resemblance between the E_G that have been calculated at GGA functional and that computed by Takeshi Kayama and his colleagues.[48] Moreover, the bandgap calculated using HSE06 is roughly equal to the theoretical value computed, which is of the order of 2.7eV, which implies the accuracy of the GGA functional of describing the electronic distribution of Mg-Py molecule than other functionals.

This is very well explained by the computed density of states (TDOS) for the pure Mg-Py molecules, as depicted in figure 4. As shown in figure 4, the TDOS of the Mg-Py molecule using GGA functional exhibits distinct bandgap energy from the TDOS calculated at HSE06 functional. We discovered that switching from HSEO6 to GGA functional causes reduction of band gaps, and that different xc functional states cause local energy levels to arise in the gap of the Mg-Py molecule, which is similar to those found in the table 1. This would

result in a change in the conductance of the Mg-Py molecule at various states of xc functional.

In addition, figure5 illustrates the absorption coefficient and reflectivity as a function of wavelength, which are the two key aspects of explaining the optical behavior of the Mg-Py molecule.

Based on the research conducted by Laxman Pandey and al[49], the isolated Mg-Py molecule's molecular orbital overlap between HO and LU may be a reason in the increased absorption spectra. As shown in figure5-(A), the magnesium-porphyrin molecule exhibits weak absorption intensities in the UV region, at GGA and HSE06 functinals. However, the Mg-Py molecule demonstrates excellent visible light absorption, with maximum intensities appearing at wavelengths of approximately 528 nm and 578 nm using HSE06 and GGA respectively. This result refers to the tiny bandgap of this molecule, which enables the fast transitions of electrons between orbitals due to its rich and powerful $pi - pi$ stacking characteristic.

DFT was used to compute the optical reflectance of the magnesium prophyrin molecle at GGA and HSE06 xc functionals. As seen in figure5-(B) the Mg-Py molecule exhibits a significant amount of reflectance between (200 nm and 380 nm) in the UV region, due to the inter-band transition (carriers absorption). On the other hand, weak reflectance intensities appeared in the visible light range, suggesting the possibility of adopting this molecule as one of the active layer's components, which would enhance our system's optical behavior upon encapsulation.

Table 1: HO, LU, Fermi level, and Bandgap energy (eV) of the pristine Mg-Py molecule.

	HO (eV)	LU (eV)	FE (eV)	E_G (eV)
GGA	-4.78	-2.79	-4.73	1.99
HSE06	-5.13	-2.58	-5.11	2.54
Exp.[48]				1.98
Theo.[46]				2.7

Organic-inorganic Mg-Py molecule confined into semiconducting single-walled nanotubes

Optoelectronic properties

In this part, we discuss the calculated optoelectronic properties of the two caracteristic configurations of the Mg-Py molecule encapsulated inside SWNT17

We note that the Mg atom is always positioned in the centre of the nanotube, and we chose a tube diameter of about 1.5nm to accommodate one Mg-Py molecule. The distance between the encapsulated component and the nanotube is predicted at 6.66 $\mathring{A}$. The generalized gradient approximation (GGA)[44] and the 6-31G(d) basis set[50] were employed in first-principles calculations based on density functional theory to investigate these computations.

Here, we explore the potential for photo induced electron transfer and excitation energy transfer from Mg-Py to SWNT17s by reference to the electronic parameters listed in table2, such as HO, LU, Fermi energy(FE) and band gap energy (E_G) for the pristine SWNT17 and hybrid nano-systems (Mg-Py@SWNT17, Mg-Py2@SWNT17). Table2 displays the Fermi level location of the empty SWNT17 and its modifications with respect to its initial position after encapsulation.

The presence of charge transfer from the Mg-Py molecule to SWNT17 can be explained by the fact that the Fermi energy of the pristine SWNT17 is higher compared to configurations with encapsulated molecules. We observe that this up-shift rises as we move from the Mg-Py molecule's front configuration inside SWNT17 to its horizontal form, which corresponds to 0.36, and 0.39eV for the hybrid nano-systems Mg-Py@SWNT17 and Mg-Py2@SWNT17, respectively. According to the order of the energies of the LU orbital in Mg-Py, the LU orbital in SWNT17s, the HO orbital in Mg-Py, and the HO orbital in SWNT17s, both the electron and hole excited in Mg-Py relax to SWNT17s, causing excitation energy transfer. With regard to the bandgap energy, we observed that the distance between HO and LU of

SWNT17 gets smaller upon encapsulation, with different positions of the Mg-Py molecule inside the nanotube, which corresponds to E_G of approximately 0.52, 0.52, and 0.49eV for the pure SWNT17, Mg-Py@SWNT17, and Mg-Py2@SWNT17 respectively. This reduction of band gaps of the hybrid systems shows the capability of the encapsulation to improve the conductivity of organic solar cell devices.

Additionally, figure6 shows the total density of states (TDOS) computed using gradient generalized approximation for pristine SWNT17, Mg-Py@SWNT17, and Mg-Py2@SWNT17 for a comprehensive knowledge of the electrical features of the enclosed hybrid systems. Since the spectrum overlap of the TDOS between Mg-Py and SWNT17s at the LU level is greater than that at the HO level, this results in excitation energy transfer, which is electron exchange via overlap of the electron wave functions between the Mg-Py (donor component) and SWNT17s (acceptor part). Hence, to increase the PCE of OSCs, this functional charge separation between the two subsystems is required. Moreover, the Mg-Py molecules' electrons may be directly stimulated to SWNT17 when the hybrid systems are exposed to light, resulting in a functional charge separation between the two subsystems that is necessary for enhancing the PCE of OSCs. In this regard, the electronic structure produced with the GGA containing Van Der Waals (vdWs) interaction is used to determine the UV-visible absorption spectra of SWNT17 and Mg-Py encapsulated hybrid systems, as shown in figure7-(A).

These hybrids exhibit a potent optical absorption in both visible light and UV regions. Since we are interested in visible light spectrum, the optical absorption edges of the enclosed systems are slightly higher than those of isolated SWNT17 because of the smaller bandgaps of the hybrids, which correspond to wavelengths of approximately 571 nm and 474 nm for Mg-Py@SWNT17 and Mg-Py2@SWNT17 respectively. Additionally, figure7-(B) displays the overall reflectance intensities of our computed systems. As can be seen, the Pristine SWNT17, Mg-Py@SWNT17, and Mg-Py2@SWNT17 all exhibited essentially the same behavior in the UV-visible light regions. The optical reflectance curves of the hybrids are slightly lower than that of isolated SWNT17 in the visible light region as well as in the

Ultraviolet range, and remained roughly the same intensities. Which demonstrate the stability of hybrids under UV-visible spectrum. Following that, using the electron energy levels and associated wave functions from the simulations of the electrical structure, we examined the real (REAL[$\epsilon(\omega)$]) and imaginary (IMG[$\epsilon(\omega)$]) components of the dielectric function throughout a wide spectrum range, from the infrared to the Visible-NUV spectral regions for the pure SWNT17 and hybrid systems as seen in figure8. The real (REAL[$\epsilon(\omega)$]) part of dielectric function (see figure8-(A)) showed a strong peak domined in the IR range at 0.5eV for the isolated SWNT17, and a weak respond is observed from the nanotube in the visible-NUV spectrum. Whereas the two hybrids showed significant changes in visible light as well as in the NUV spectral regions in comparison with the single-walled carbon nanotube, after encapsulation, particularly for the hybrid Mg-Py2@SWNT17, where the Mg-Py molecule is positioned vertically inside the nanotube, displays high peaks in the visible light spectrum, at energies of around 2.4 and 3.3eV. Generally, the two hybrids showed identical features due to the similarities in the chemical structure between Mg-Py@SWNT17 and Mg-Py2@SWNT17. Regarding the imaginary (IMG[$\epsilon(\omega)$]) part of the dielectric function, which is related to the interband transitions corresponding to the radiation absorption by electrons in the occupied valance bands below the Fermi level, the isolated SWNT17 produced primarily the same characteristics as the real part, It is depicted in figure8-(B), and demonstrated the predominance of significant peaks in the infrared region at energies of roughly 0.56, 0.7, and 1.08 eV, on the opposite side low peaks in the visible-NUV spectrum can be detected. In contrast, after encapsulation, both hybrids exhibit a significant intensity variation in the visible-NUV spectral region, where strong peaks are dominated. This is especially true for the hybrid Mg-Py@SWNT17, in which the Mg-Py molecule is positioned in front inside the nanotube and exhibits an overall domination of strong peaks at energies of about 2.25, 2.57, and 3.41eV. Whereas, the other hybrid, in which the molecule is positioned vertically within the nanotube, showed a strong respond in the near ultraviolat spectrum at energy of around 4.12ev, and disappearance of high intensity peaks has been noticed in the Infrared

range. the latter suggests that Mg-Py encapsulated systems can be used in electro-optical devices, particularly in OSCs. These two factors, along with the peculiar optical properties of semiconducting carbon nanotubes, make them potential candidates for use in OSCs. Then, according to the optical calculations, the absorption of SWNTs for the solar spectrum is improved upon encapsulation, due to the wider absorption band of the hybrids in the visible-light region, which makes these hybrids a good candidate in OSCs devices. After all, we believe that using filled semiconduction SWNTs with organic-inorganic molecules that exhibit type II heterojunctions as a light harvester and charge transport in the active layer may lead to improved PCE and long-term stability for more qualified OSCs.

Table 2: Bandgaps energy (E_G) ,HO ,LU and fermi energy (FE) of pure SWNT17, Mg-Py@SWNT17 and Mg-Py2@SWNT17 nano-hybrid systems.

	HO	LU	FE	E_G
SWNT17	-1.04	-0.52	-1.30	0.52
Mg-Py@SWNT17	-1.00	-0.48	-1.94	0.52
Mg-Py2@SWNT17	-0.92	-0.42	-0.91	0.49

Conclusion

In this study, the optoelectronic distributions of single Mg-Py molecules and Mg-Py enclosed nano-systems were described using the DFT framework. First, the optoelectronic properties for the isolated magnesium-porphyrin molecule using GGA and HSE06 xc functional have been calculated, the results are excellent both in terms of optical characteristics and the electric field. We show also that the GGA used to achieve the narrow bandgap is more accurate than the other functionals, suggestion that changing the functional causes variations in the conductivities behavior. The optical absorption calculation revealed a substantial response from the Mg-Py molecule in the visible light area, demonstrating the possibility of using this molecule as one of the active layer components. Then, using the DFT framework,

we estimated the electrical and optical characteristics of the encapsulated hybrid systems (Mg-Py@SWNT17 and Mg-Py2@SWNT17), and in order to identify the CT and its direction in our hybrids, we show that the rising FE of SWNT17 following encapsulation, led to a CT connection from the Mg-Py molecule to SWNT17, suggesting that the hybrids contain type-II band alignment.

Acknowledgement

The work was supported by Moulay Ismail University Research Support (13-16) and Comisión Nacional de Investigación Científica y Tecnológica (CONICYT)-Fondo Nacional de Desarrollo Científico y Tecnológico (FONDECYT) Posdoctodado 2020 Nº 3200046. JML acknowledges support from Financiamiento basal para centros científicos y tecnológicos de excelencia AFB180001.

References

(1) Ondrey, G. Organic solar cells. *Chemical Engineering* **2011**, *118*, 13–15.

(2) McMeekin, D. P.; Wang, Z.; Rehman, W.; Pulvirenti, F.; Patel, J. B.; Noel, N. K.; Johnston, M. B.; Marder, S. R.; Herz, L. M.; Snaith, H. J. Crystallization Kinetics and Morphology Control of Formamidinium–Cesium Mixed-Cation Lead Mixed-Halide Perovskite via Tunability of the Colloidal Precursor Solution. *Advanced Materials* **2017**, *29*, 1607039.

(3) Guerra, V. L.; Altamura, D.; Trifiletti, V.; Colella, S.; Listorti, A.; Giannuzzi, R.; Pellegrino, G.; Condorelli, G. G.; Giannini, C.; Gigli, G., et al. Implications of TiO 2 surface functionalization on polycrystalline mixed halide perovskite films and photovoltaic devices. *Journal of Materials Chemistry A* **2015**, *3*, 20811–20818.

(4) Green, M. A.; Bremner, S. P. Energy conversion approaches and materials for high-efficiency photovoltaics. *Nature materials* **2017**, *16*, 23–34.

(5) Heeger, A. J. 25th anniversary article: bulk heterojunction solar cells: understanding the mechanism of operation. *Advanced materials* **2014**, *26*, 10–28.

(6) Guan, L.; Shi, Z.; Li, M.; Gu, Z. Ferrocene-filled single-walled carbon nanotubes. *Carbon* **2005**, *43*, 2780–2785.

(7) Gimenez-Lopez, M. d. C.; La Torre, A.; Fay, M. W.; Brown, P. D.; Khlobystov, A. N. Assembly and magnetic bistability of Mn3O4 nanoparticles encapsulated in hollow carbon nanofibers. *Angewandte Chemie* **2013**, *125*, 2105–2108.

(8) Manzetti, S. Molecular and crystal assembly inside the carbon nanotube: encapsulation and manufacturing approaches. *Advances in Manufacturing* **2013**, *1*, 198–210.

(9) Meunier, V.; Sumpter, B. G. Amphoteric doping of carbon nanotubes by encapsulation of organic molecules: electronic properties and quantum conductance. *The Journal of chemical physics* **2005**, *123*, 024705.

(10) Dinadayalane, T.; Gorb, L.; Simeon, T.; Dodziuk, H. Cumulative π-π interaction triggers unusually high stabilization of linear hydrocarbons inside the single-walled carbon nanotube. *International Journal of Quantum Chemistry* **2007**, *107*, 2204–2210.

(11) Cheng, P.; Li, G.; Zhan, X.; Yang, Y. Next-generation organic photovoltaics based on non-fullerene acceptors. *Nature Photonics* **2018**, *12*, 131–142.

(12) Zhang, J.; Tan, H. S.; Guo, X.; Facchetti, A.; Yan, H. Material insights and challenges for non-fullerene organic solar cells based on small molecular acceptors. *Nature Energy* **2018**, *3*, 720–731.

(13) Gao, K.; Kan, Y.; Chen, X.; Liu, F.; Kan, B.; Nian, L.; Wan, X.; Chen, Y.; Peng, X.;

Russell, T. P., et al. Low-bandgap porphyrins for highly efficient organic solar cells: materials, morphology, and applications. *Advanced Materials* **2020**, *32*, 1906129.

(14) Zhang, M.; Zhu, L.; Zhou, G.; Hao, T.; Qiu, C.; Zhao, Z.; Hu, Q.; Larson, B. W.; Zhu, H.; Ma, Z., et al. Single-layered organic photovoltaics with double cascading charge transport pathways: 18% efficiencies. *Nature communications* **2021**, *12*, 1–10.

(15) Isikgor, F.; Nugraha, M.; Yengel, E.; Harrison, G.; Hallani, R.; El Labban, A.; Faber, H.; Ma, C.; Zheng, X.; Subbiah, A., et al. Self-assembled Monolayer Enables HTL-free Organic Solar Cells with 18% Efficiency and Improved Operational Stability. *ACS Energy Lett* **2020**, *5*, 2935.

(16) Wageh, S.; Raïssi, M.; Berthelot, T.; Laurent, M.; Rousseau, D.; Abusorrah, A. M.; Al-Hartomy, O. A.; Al-Ghamdi, A. A. Digital printing of a novel electrode for stable flexible organic solar cells with a power conversion efficiency of 8.5%. *Scientific Reports* **2021**, *11*, 1–16.

(17) NREL, N. Best research-cell efficiencies. *National Renewable Energy Laboratory: Golden, Colorado* **2019**,

(18) Polman, A.; Knight, M.; Garnett, E. C.; Ehrler, B.; Sinke, W. C. Photovoltaic materials: Present efficiencies and future challenges. *Science* **2016**, *352*, aad4424.

(19) Chenouf, J.; Boutahir, M.; Mejía-López, J.; Rahmani, A.; Fakrach, B.; Chadli, H.; Rahmani, A. Predicting the structure configuration and Raman analysis of caffeine molecules encapsulated into single-walled carbon nanotubes: Evidence for charge transfer. *Solar Energy* **2022**, *232*, 204–211.

(20) Waldauf, C.; Scharber, M. C.; Schilinsky, P.; Hauch, J. A.; Brabec, C. J. Physics of organic bulk heterojunction devices for photovoltaic applications. *Journal of applied physics* **2006**, *99*, 104503.

(21) Blackburn, J. L. Semiconducting single-walled carbon nanotubes in solar energy harvesting. *ACS Energy Letters* **2017**, *2*, 1598–1613.

(22) Bachilo, S. M.; Strano, M. S.; Kittrell, C.; Hauge, R. H.; Smalley, R. E.; Weisman, R. B. Structure-assigned optical spectra of single-walled carbon nanotubes. *science* **2002**, *298*, 2361–2366.

(23) Cataldo, S.; Salice, P.; Menna, E.; Pignataro, B. Carbon nanotubes and organic solar cells. *Energy & Environmental Science* **2012**, *5*, 5919–5940.

(24) Jeon, I.; Matsuo, Y.; Maruyama, S. Single-walled carbon nanotubes in solar cells. *Single-walled carbon nanotubes* **2019**, 271–298.

(25) Kataura, H.; Kumazawa, Y.; Maniwa, Y.; Umezu, I.; Suzuki, S.; Ohtsuka, Y.; Achiba, Y. Optical properties of single-wall carbon nanotubes. *Synthetic metals* **1999**, *103*, 2555–2558.

(26) Keru, G.; Ndungu, P. G.; Nyamori, V. O. A review on carbon nanotube/polymer composites for organic solar cells. *International Journal of Energy Research* **2014**, *38*, 1635–1653.

(27) Bhatia, R.; Kumar, L. Functionalized carbon nanotube doping of P3HT: PCBM photovoltaic devices for enhancing short circuit current and efficiency. *Journal of Saudi Chemical Society* **2017**, *21*, 366–376.

(28) Gong, M.; Shastry, T. A.; Cui, Q.; Kohlmeyer, R. R.; Luck, K. A.; Rowberg, A.; Marks, T. J.; Durstock, M. F.; Zhao, H.; Hersam, M. C., et al. Understanding Charge Transfer in Carbon Nanotube–Fullerene Bulk Heterojunctions. *ACS Applied Materials & Interfaces* **2015**, *7*, 7428–7435.

(29) Mehlenbacher, R. D.; Wang, J.; Kearns, N. M.; Shea, M. J.; Flach, J. T.; McDonough, T. J.; Wu, M.-Y.; Arnold, M. S.; Zanni, M. T. Ultrafast exciton hopping

observed in bare semiconducting carbon nanotube thin films with two-dimensional white-light spectroscopy. *The journal of physical chemistry letters* **2016**, *7*, 2024–2031.

(30) Arias, D. H.; Sulas-Kern, D. B.; Hart, S. M.; Kang, H. S.; Hao, J.; Ihly, R.; Johnson, J. C.; Blackburn, J. L.; Ferguson, A. J. Effect of nanotube coupling on exciton transport in polymer-free monochiral semiconducting carbon nanotube networks. *Nanoscale* **2019**, *11*, 21196–21206.

(31) Flach, J. T.; Wang, J.; Arnold, M. S.; Zanni, M. T. Providing Time to Transfer: Longer Lifetimes Lead to Improved Energy Transfer in Films of Semiconducting Carbon Nanotubes. *The journal of physical chemistry letters* **2020**, *11*, 6016–6024.

(32) Wang, J.; Peurifoy, S. R.; Bender, M. T.; Ng, F.; Choi, K.-S.; Nuckolls, C.; Arnold, M. S. Non-fullerene acceptors for harvesting excitons from semiconducting carbon nanotubes. *The Journal of Physical Chemistry C* **2019**, *123*, 21395–21402.

(33) Bindl, D. J.; Shea, M. J.; Arnold, M. S. Enhancing extraction of photogenerated excitons from semiconducting carbon nanotube films as photocurrent. *Chemical Physics* **2013**, *413*, 29–34.

(34) Shea, M. J.; Wang, J.; Flach, J. T.; Zanni, M. T.; Arnold, M. S. Less severe processing improves carbon nanotube photovoltaic performance. *APL Materials* **2018**, *6*, 056104.

(35) Mallajosyula, A. T.; Nie, W.; Gupta, G.; Blackburn, J. L.; Doorn, S. K.; Mohite, A. D. Critical role of the sorting polymer in carbon nanotube-based minority carrier devices. *ACS nano* **2016**, *10*, 10808–10815.

(36) Littler, B. J.; Ciringh, Y.; Lindsey, J. S. Investigation of conditions giving minimal scrambling in the synthesis of trans-porphyrins from dipyrromethanes and aldehydes. *The Journal of Organic Chemistry* **1999**, *64*, 2864–2872.

(37) Leong, W. L.; Welch, G. C.; Kaake, L. G.; Takacs, C. J.; Sun, Y.; Bazan, G. C.; Heeger, A. J. Role of trace impurities in the photovoltaic performance of solution processed small-molecule bulk heterojunction solar cells. *Chemical Science* **2012**, *3*, 2103–2109.

(38) Ogumi, K.; Nakagawa, T.; Okada, H.; Sakai, R.; Wang, H.; Matsuo, Y. Substituent effects in magnesium tetraethynylporphyrin with two diketopyrrolopyrrole units for bulk heterojunction organic solar cells. *Journal of Materials Chemistry A* **2017**, *5*, 23067–23077.

(39) Lu, Y.; Xiao, Z.; Yuan, Y.; Wu, H.; An, Z.; Hou, Y.; Gao, C.; Huang, J. Fluorine substituted thiophene–quinoxaline copolymer to reduce the HOMO level and increase the dielectric constant for high open-circuit voltage organic solar cells. *Journal of Materials Chemistry C* **2013**, *1*, 630–637.

(40) Mahmood, A.; Hu, J.-Y.; Xiao, B.; Tang, A.; Wang, X.; Zhou, E. Recent progress in porphyrin-based materials for organic solar cells. *Journal of Materials Chemistry A* **2018**, *6*, 16769–16797.

(41) Eichkorn, K.; Treutler, O.; Oehm, H.; Häser, M.; Ahlrichs, R. Auxiliary basis sets to approximate Coulomb potentials (Chem. Phys. Letters 240 (1995) 283-290). *Chemical Physics* **1995**, *242*, 652–660.

(42) Eichkorn, K.; Treutler, O. H.÷ hm, M. H‰ ser, R. Ahlrichs. *Chem. Phys. Lett* **1995**, *240*, 283.

(43) Kresse, G.; Furthmüller, J. Efficient iterative schemes for ab initio total-energy calculations using a plane-wave basis set. *Physical review B* **1996**, *54*, 11169.

(44) Perdew, J. P.; Burke, K.; Ernzerhof, M. Generalized gradient approximation made simple. *Physical review letters* **1996**, *77*, 3865.

(45) Grimme, S. Semiempirical GGA-type density functional constructed with a long-range dispersion correction. *Journal of computational chemistry* **2006**, *27*, 1787–1799.

(46) Rubio, M.; Roos, B. O.; Serrano-Andrés, L.; Merchán, M. Theoretical study of the electronic spectrum of magnesium-porphyrin. *The Journal of chemical physics* **1999**, *110*, 7202–7209.

(47) Hasegawa, J.; Ozeki, Y.; Ohkawa, K.; Hada, M.; Nakatsuji, H. Theoretical study of the excited states of chlorin, bacteriochlorin, pheophytin a, and chlorophyll a by the SAC/SAC- CI method. *The Journal of Physical Chemistry B* **1998**, *102*, 1320–1326.

(48) Koyama, T.; Sugiura, J.; Koishi, T.; Ohashi, R.; Asaka, K.; Saito, T.; Gao, Y.; Okada, S.; Kishida, H. Excitation energy transfer by electron exchange via two-step electron transfer between a single-walled carbon nanotube and encapsulated magnesium porphyrin. *The Journal of Physical Chemistry C* **2020**, *124*, 19406–19412.

(49) Pandey, L.; Risko, C.; Norton, J. E.; Bredas, J.-L. Donor–acceptor copolymers of relevance for organic photovoltaics: A theoretical investigation of the impact of chemical structure modifications on the electronic and optical properties. *Macromolecules* **2012**, *45*, 6405–6414.

(50) Rassolov, V. A.; Ratner, M. A.; Pople, J. A.; Redfern, P. C.; Curtiss, L. A. 6-31G* basis set for third-row atoms. *Journal of Computational Chemistry* **2001**, *22*, 976–984.

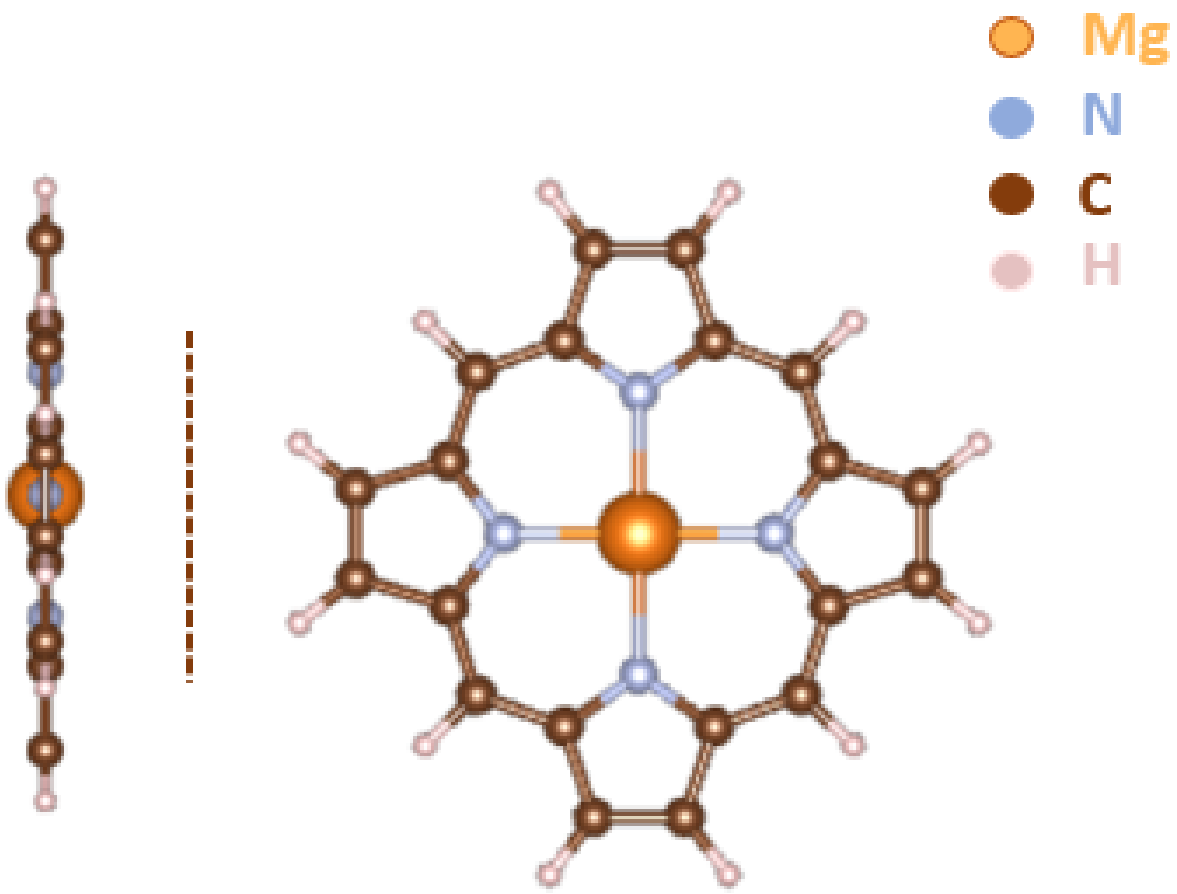

Figure 1: Structure presentation of magnesium Porphyrin(Mg-Py) molecule

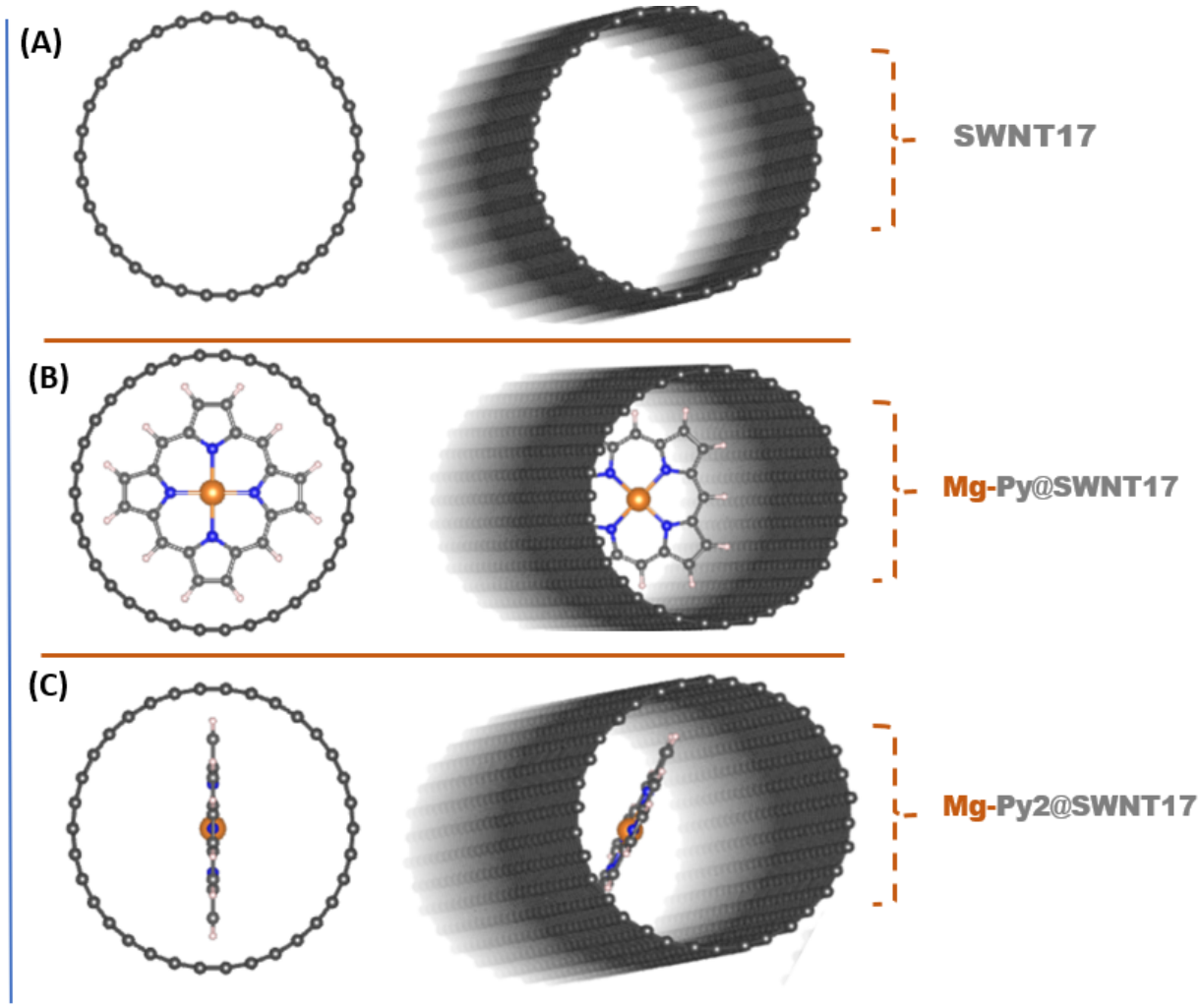

Figure 2: Schematic representation of : (A) The pure SWNT17. (B) Mg-Py@SWNT17. (C) Mg-Py2@SWNT17.

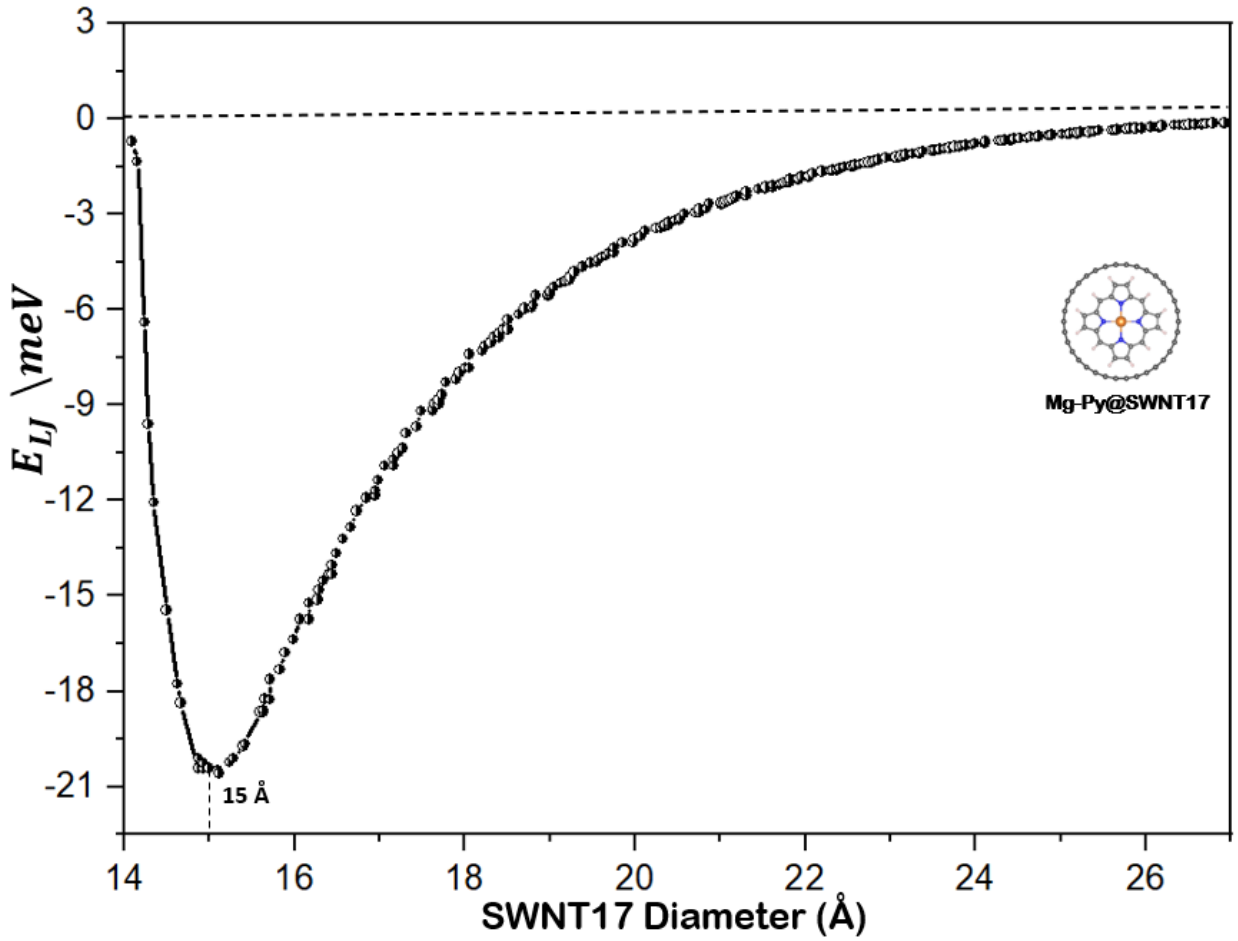

Figure 3: Minimizing the energy calculations of Mg-Py@SWNT17 across various diameters.

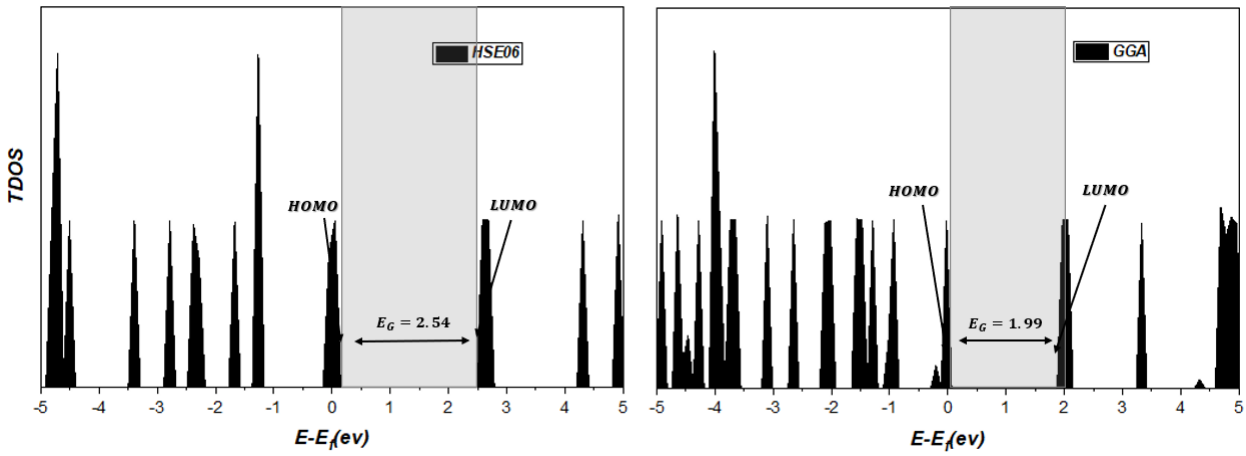

Figure 4: Total density of states (TDOS) of isolated Mg-Py molecule using GGA and HSE06 xc functionals.

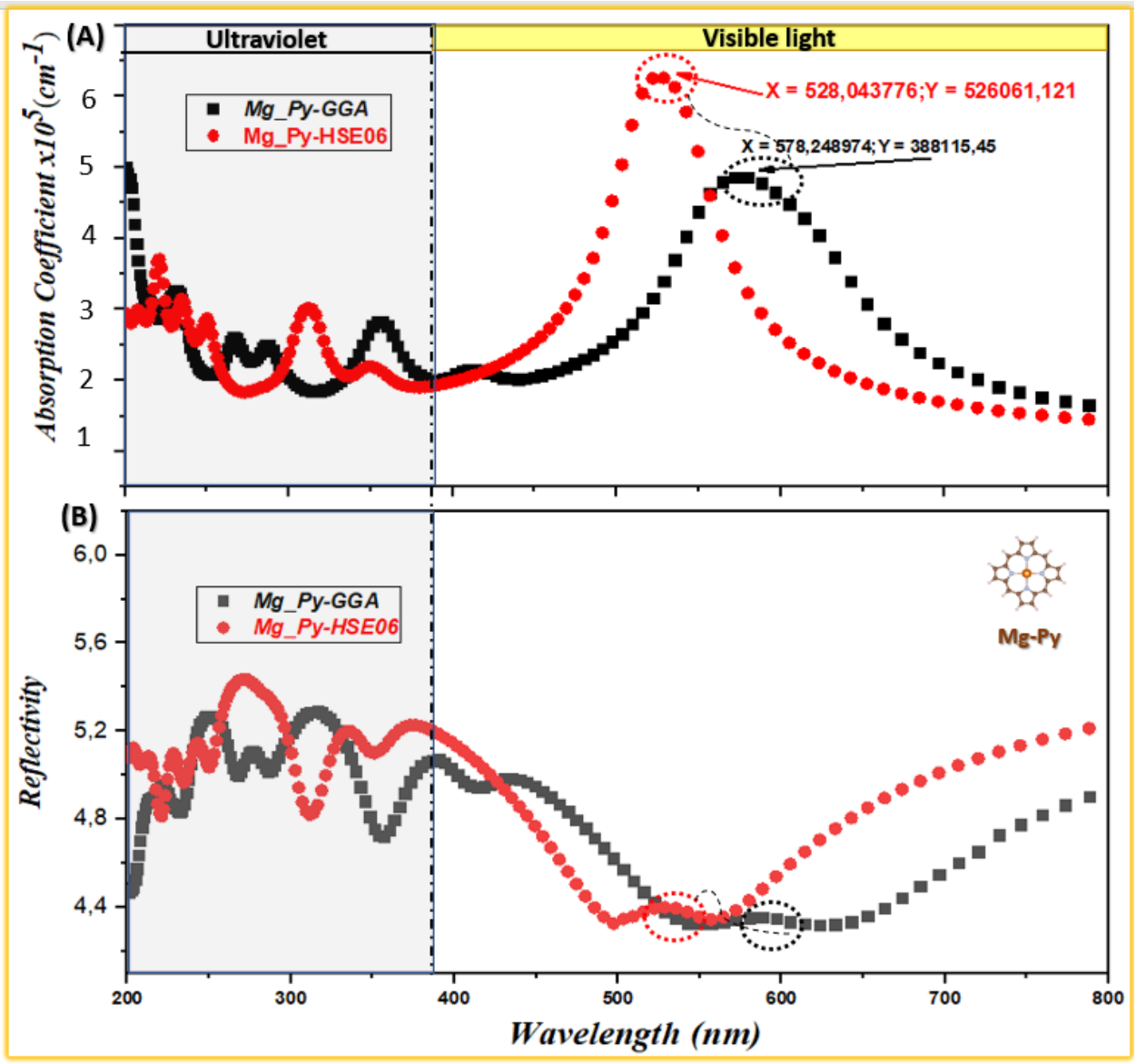

Figure 5: Optical characteristics of isolated Mg-Py molecule using GGA and HSE06 xc functionals: (A) Absorption coefficient spectra ; (B) Reflectivity spectrum.

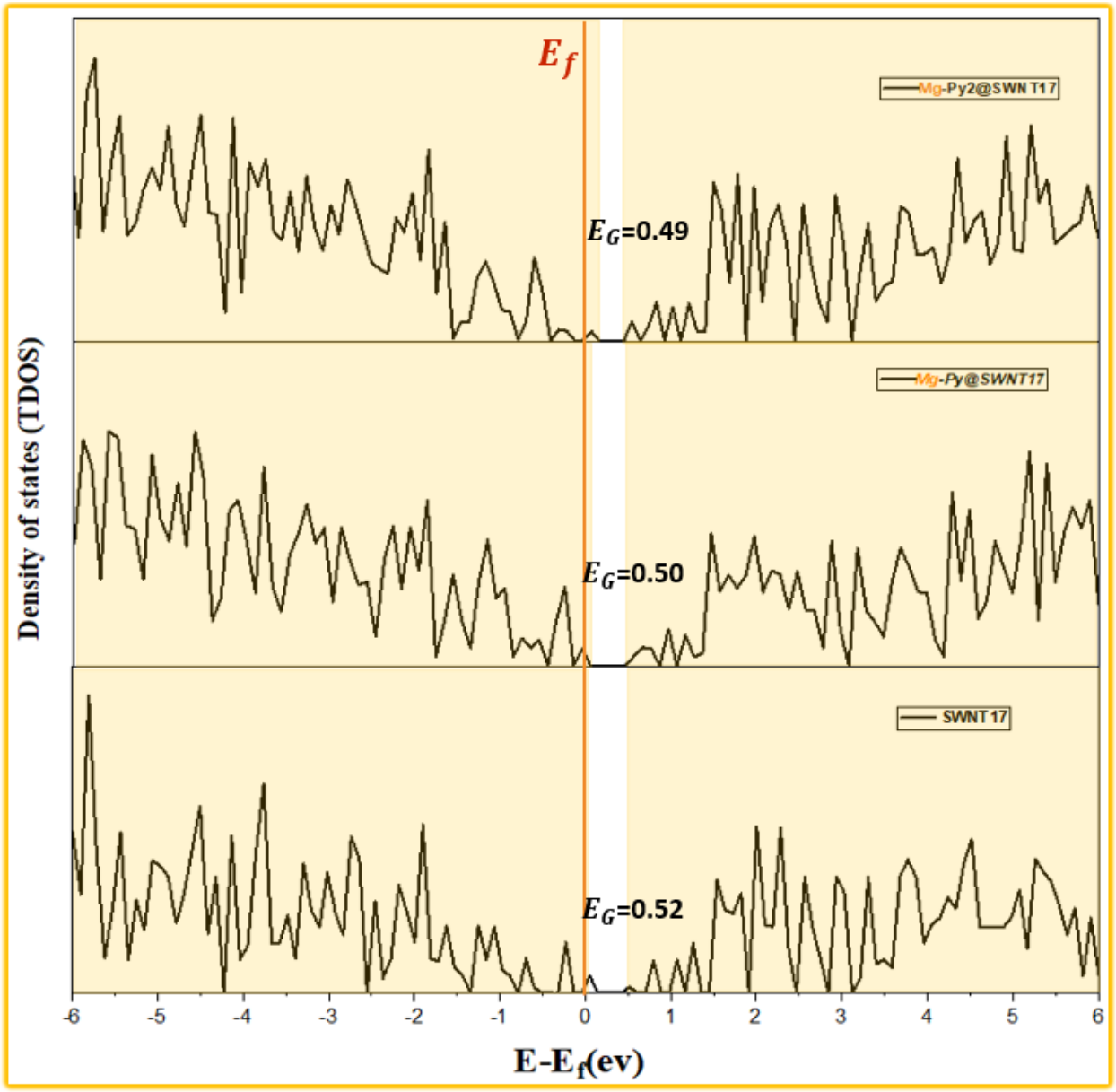

Figure 6: Total density of states (TDOS) illustration of pristine SWNT17, Mg-Py@SWNT17 and Mg-Py2@SWNT17 haybrid nano-system using GGA functional.

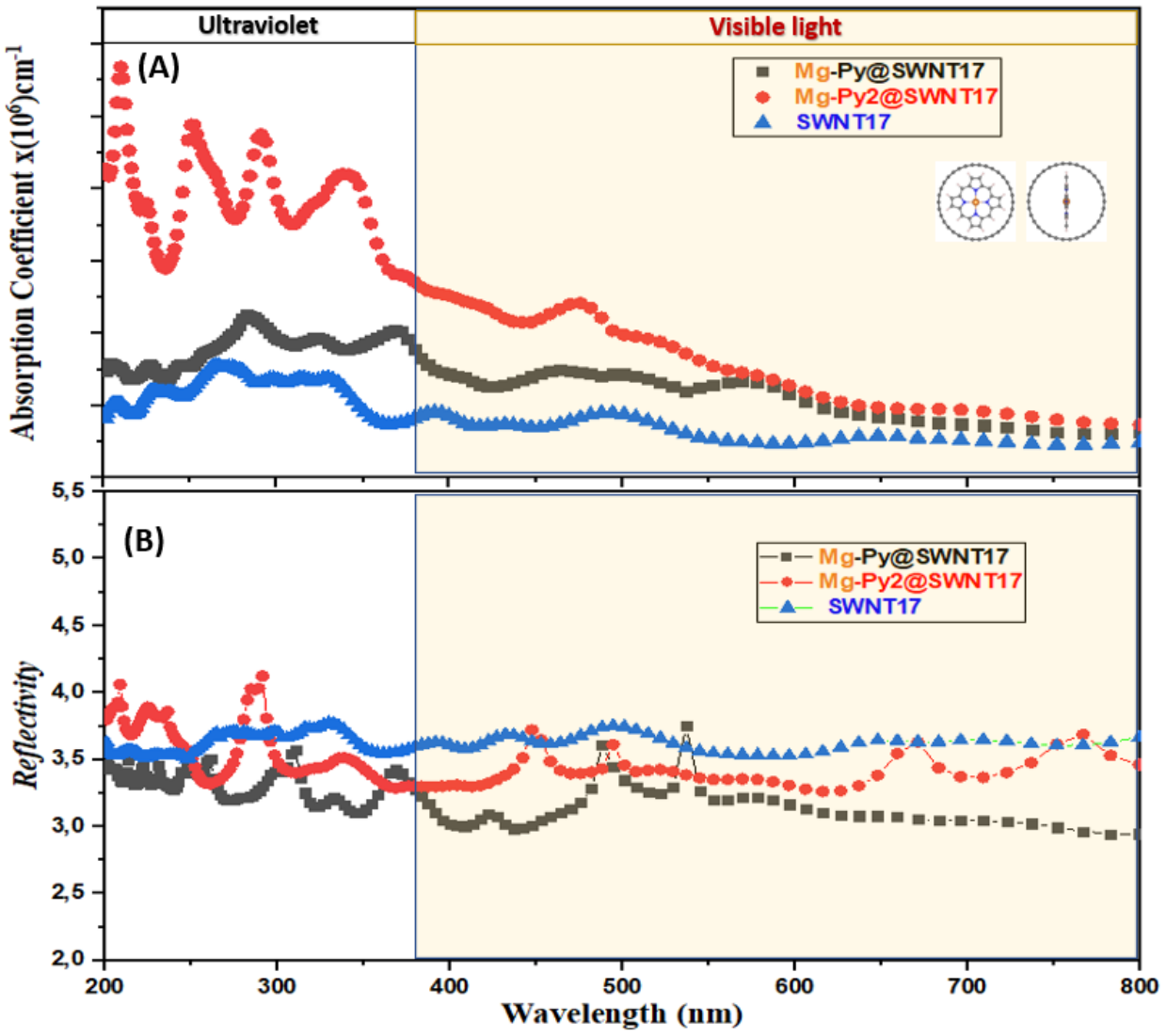

Figure 7: Optical properties of the pristine SWNT17 (bleu triangles), Mg-Py@SWNT17 (black squares), and Mg-Py2@SWNT17 (red circles) nano-hybrid systems using GGA functional: (A) Absorption coefficient spectra.(B) Reflectivity spectrum.

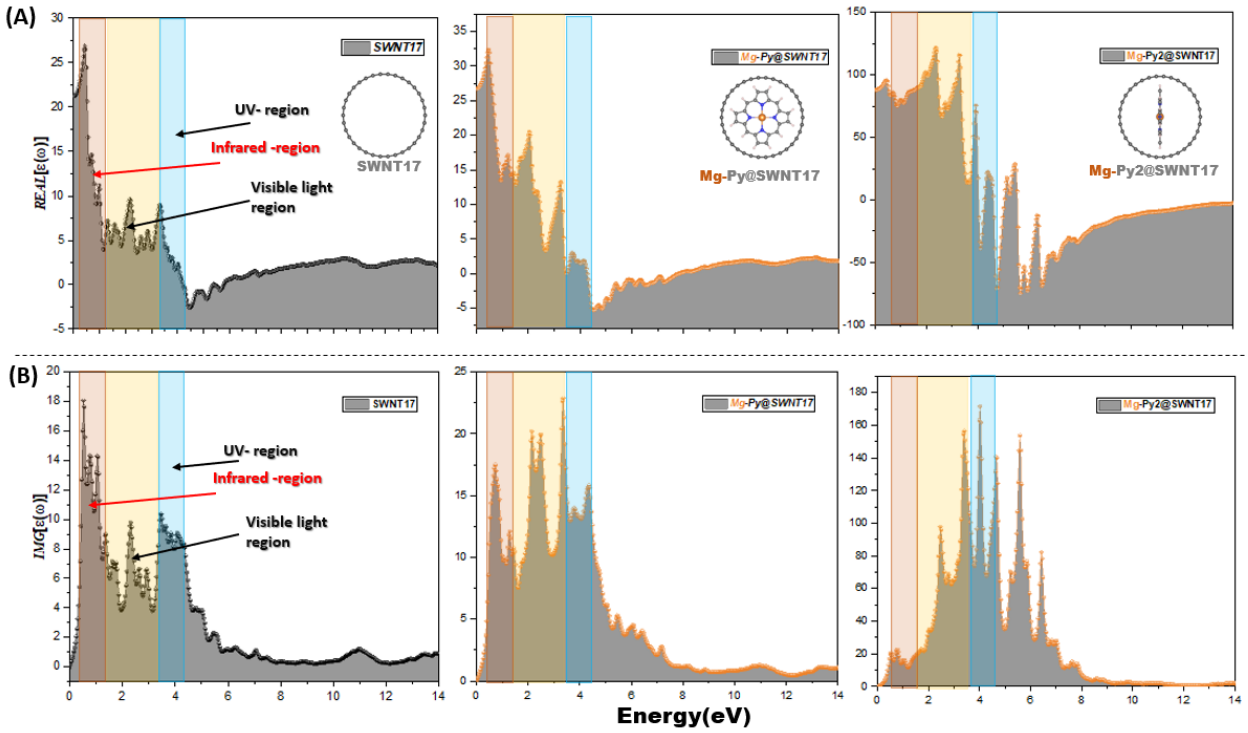

Figure 8: Dielectric functions representation of pristine SWNT17, Mg-Py@SWNT17 and Mg-Py2@SWNT17: (A) Real part (REAL[$\epsilon(\omega)$]). (B) Imaginary part (IMG[$\epsilon(\omega)$]). In red, yellow and blue rectangles we seprate the infrared, visible and UV regions to help discussions.